UCRL- 92811
PREPRINT

Development of a Novel Soft X-ray Source for Laboratory Applications

D. G. Stearns

This paper was prepared for submittal to
Nuclear Methods and Instrumentation

June 12, 1985

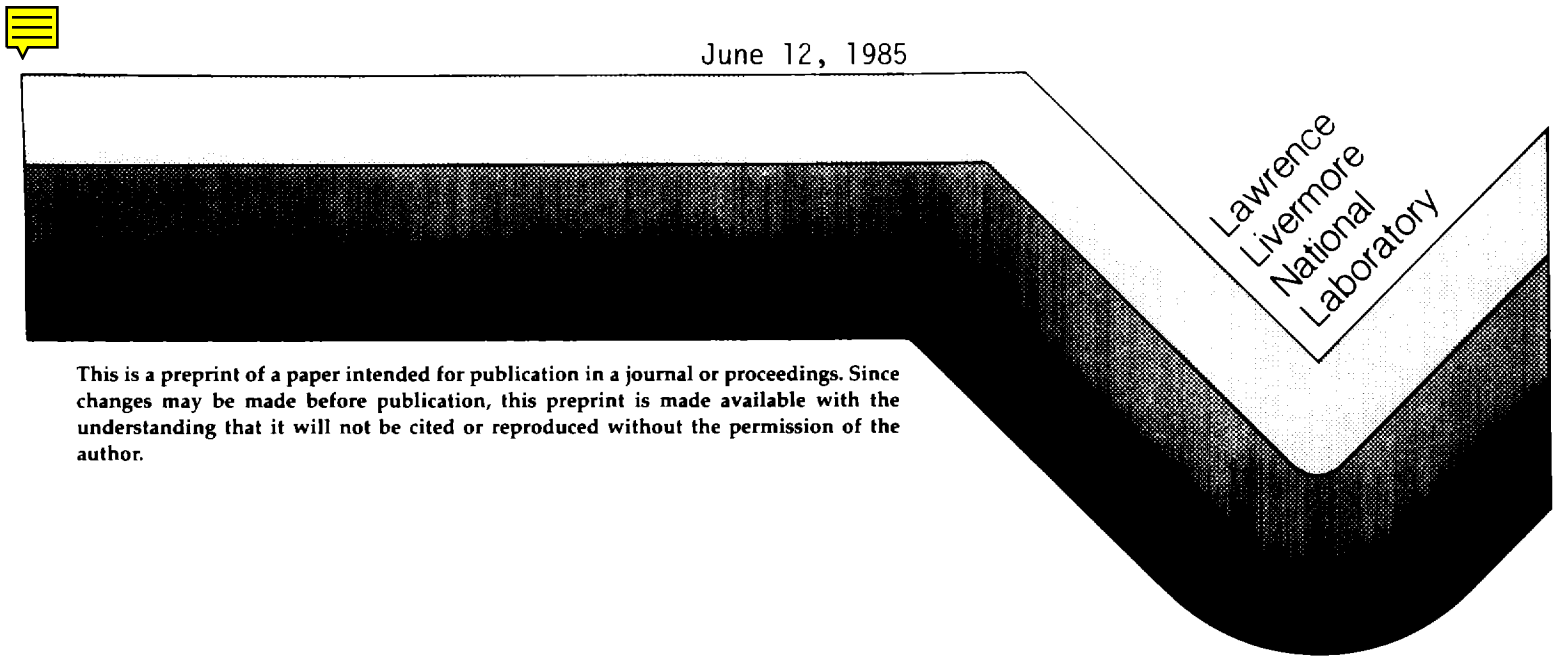

Development of a Novel Soft X-ray Source for Laboratory Applications*

D. G. Stearns
Lawrence Livermore National Laboratory

ABSTRACT

A new soft x-ray source has been developed and characterized. X-rays are generated by the illumination of a multialkali photocathode with visible light to produce electrons that are accelerated onto a thin metal film anode. The novel feature of the design is that the photocathode and anode are in close proximity so that the x-ray emission is a spatial and temporal replica of the input light signal. Measurements of the x-ray emission brightness, energy spectrum and minimum source size are presented, and some unique applications of the new source are discussed.

*Work performed under the auspices of the U. S. Department of Energy by the Lawrence Livermore National Laboratory under contract number W-7405-ENG-48.

Design.

This paper describes the development and characterization of a new soft x-ray source: the x-ray diode source (XRDS). The XRDS is a compact disk-shaped device, approximately two inches in diameter and one inch wide. A schematic illustration of the XRDS is shown in Figure 1. The simple design incorporates an extended-red multialkali transmission photocathode mounted in close proximity (3 mm) to a transmission anode. The photocathode is deposited on a glass input window using a process that reduces the sheet resistance to less than 1 kohm/square. The tube is permanently sealed under high vacuum to avoid contamination of the photocathode. The anode structure consists of a thin film of metal deposited on a 5-mil-thick beryllium output window. The window is 1 cm in diameter, which defines a maximum source area of 0.8 cm^2. The XRDS is specified to operate at a maximum DC voltage of 12 kV.

X-rays are produced by illuminating the photocathode through the glass window with visible or near-infra-red light. The photoelectrons are accelerated across the gap and bombard the anode, generating characteristic x-ray and bremstrahlung emission which is transmitted through the beryllium output window. Two XRDS's have been fabricated to date, with thin metal film anodes of titanium (4000Å) and gold (500Å). The thickness of the metal films has been chosen to be greater than the range of a 10 keV electron in these materials. The gold film has been kept thin to minimize self-absorption of the x-rays.

A unique feature of the XRDS is that, owing to the proximity focus geometry, the x-ray emission is intimately related to the input light signal. In particular, the spatial configuration of the x-ray source is a replica of the illumination pattern on the photocathode. Similarly,

any temporal modulation of the input light signal is directly reproduced in the x-ray emission.

Characterization.

This section describes the characterization of the XRDS, including measurements of the emission brightness, energy spectrum and minimum source size (point spread function). Further evaluation of the XRDS, including an investigation of the temporal response, is currently in progress.

The configuration of the test station used to evaluate the XRDS is sketched in Figure 2. The XRDS was mounted on a flange located at one end of a vacuum flight tube. A glass window in the flange permitted the XRDS to be illuminated with a helium-neon laser (λ = 632 nm) from outside the vacuum. The x-rays emitted by the XRDS were detected with an x-ray CCD camera that was mounted at the other end of the flight tube. The camera was custom built at MIT and has been described previously.[1] It incorporates a front-illuminated virtual phase CCD made by Texas Instruments. The CCD contains an array of 584 by 390 pixels, each of dimension 22 x 22 microns. During operation the CCD is cooled to $\sim$-60C and the device is scanned slowly to reduce the total noise to $\sim$20 electrons/pixel, which is well below the signal produced by a single x-ray.[2] The calculated x-ray detection efficiency of the CCD is shown in Figure 3. The combination of low noise and high efficiency makes the CCD camera ideally-suited for experiments where both imaging and photometric analysis are required. A 5-mil-thick beryllium window was installed in front of the camera to prevent scattered light from reaching the CCD.

The XRDS emission spectrum was measured with the photocathode uniformly illuminated at an intensity level of $\sim$0.1 mW/cm^2. The current generated between the photocathode and the anode was monitored, and the photocathode efficiencies at 632 nm were found to be 25 uA/mW (Ti-anode XRDS) and 32 uA/mW (Au-anode XRDS). X-rays were collected by the CCD camera for an exposure time of several milliseconds, controlled by an electronic shutter located in the laser beam path. The x-rays were detected as single events in a 200 x 200 pixel sub-array on the CCD. The location of the sub-array was chosen to be as close as possible to the on-chip output amplifier, in order to minimize charge spreading during readout. X-ray spectra were obtained by constructing a histogram of the single x-ray events as a function of the charge deposited in the CCD pixel. Events in which the charge was distributed between two or more pixels were discarded. The spectra were subsequently adjusted to take into account the detection efficiency of the CCD and transmission through the beryllium window.

The x-ray emission spectra of the titanium and gold-anode XRDS's operating at 10 kV are shown in Figure 4. The energy resolution at 4.5 keV is approximately 200 eV. The titanium emission spectrum is dominated by the K-alpha and K-beta lines at 4.5 keV, which are not separately resolved. In contrast, the gold spectrum exhibits broadband bremsstrahlung emission across the entire 2-10 keV range, with an additional contribution from the gold M-band transitions at 2.0-2.4 keV.

The brightness of the x-ray emission is indicated on the vertical scale of the spectra in Figure 4. The ordinate values have been normalized to an anode current of 1 mA and an emission energy bandwidth of 1 keV. The brightness was determined by integrating the total number

of x-rays detected in the sub-array during an exposure. In the case of the titanium-anode XRDS approximately 50% of the total x-ray power is emitted into the K lines. The ratio of the power associated with the photoelectrons (as determined from the anode current and operating voltage) to the x-ray power emitted into the titanium K lines implies a conversion efficiency into the K lines of 3×10^{4}.

The input light intensity was varied in order to determine the maximum level of illumination at which the photocathode could be safely operated. In DC operation the anode current density was observed to be stable up to a level of $\sim$5 mA/cm^2. At higher illumination the anode current was found to decrease in time, which is probably due to degradation of the photocathode associated with resistive heating. This implies that the XRDS can be safely operated at an emission brightness of up to $\sim 10^{12}$ phot/sec-cm^2-srad.

The x-ray source spot of the titanium-anode XRDS was imaged onto the CCD camera using a pinhole of 50 microns in diameter at a magnification of 10. The purpose of this measurement was to investigate the spatial dispersion of the photoelectron beam inside the XRDS and hence determine the minimum source size. Figure 5a shows the image of the source spot generated by projecting a 25 micron spot of light onto the photocathode and operating the XRDS at 10 kV. The spreading that occurs in the transfer of the input spot to the output spot is associated with the transverse energy E_t of the photoelectrons as they are initially emitted from the photocathode. It has been shown[3] that the transverse energy distribution $P(E_t)$ of the electrons emitted from a multi-alkali (Sb-K-Na-Cs) photocathode can be described by

$$P(E_t) = P(0)\exp(-E_t/\bar{E}_t) \qquad (1)$$

where $\bar{E}_t$ = 0.076 eV for excitation at 600 nm. A point illumination of the photocathode produces an x-ray source spot S(r) having a Gaussian profile,

$$S(r)=S(0)\exp-(r^2/\sigma^2) \qquad (2)$$

where

$$\sigma^2 = 4d^2\bar{E}_t/eV \qquad (3)$$

Here d is the gap width, e is an electric charge and V is the operating voltage. In the case of the XRDS operating at 10 kV, equation (2) predicts a point response of σ = 16 microns. Figure 5b shows a lineout across a diameter of the image in Figure 5a. The dashed line represents the best fit to the lineout generated by convoluting the point response function (2) with a 25-micron input spot and a 50-micron pinhole. The best fit is obtained using σ = 20 microns. This implies that the minimum source size of the XRDS, achieved by illuminating the photocathode at a single point, is a Gaussian spot with a full width at half maximum of 33 microns. The average transverse energy of the photoelectrons generated at 632 nm is found to be $\bar{E}_t$ = 1.1 eV.

Applications.

It is instructive to compare the XRDS with a conventional laboratory x-ray source. As an example, Reference 4 describes a typical bright laboratory source. This source produces x-rays by bombarding a water-cooled anode with a focussed electron beam that is generated from a hot filament. Table 1 compares some of the operating parameters of this conventional source to the XRDS. The conventional source can be up to 100 times brighter than the XRDS. However it is limited to a minimum

source spot size of 1-10 mm^2, and hence must be operated at high power. In contrast, the XRDS can have a very small source size, making it possible to achieve high brightness at a low power level. The absence of water-cooling and high power voltage supplies makes the XRDS much simpler to operate and to incorporate into laboratory experiments. In applications where source brightness is important, and not just total x-ray flux, the XRDS is a desirable alternative to the conventional source.

The usefulness of the XRDS, however, extends beyond conventional laboratory applications. The unique capability of directly controlling the x-ray emission through the input light signal provides for some exciting new applications. As an example, when an image is projected onto the photocathode, a replica of the pattern is produced as the x-ray source. Hence it is possible to generate x-ray emission in complex geometric patterns. In particular, three dimensional coded imaging can be performed by generating a coded source such as a Fresnel zoneplate pattern.[5] The object to be studied is placed between the XRDS and the detector as depicted in Figure 6a, and a coded image of the object is produced on the film. The three dimensional real space image can be reconstructed digitally, or by using standard holographic techniques.

The temporal modulation of the x-ray emission via the input light signal leads to novel applications such as phase-sensitive x-ray detection as depicted in Figure 6b. The intensity of the input light signal is modulated sinusoidally at frequencies ranging up to $\sim$1 MHz using an acousto-optic modulator. Weak x-ray signals, such as the higher-order reflections from multilayer mirrors, can be analyzed in phase with the reference frequency to improve the signal-to-noise by many orders of magnitude.

As an extreme example of temporal modulation, it should be possible to generate ultra-short x-ray pulses by applying picosecond light pulses to the XRDS input. Figure 6c illustrates how the XRDS can be used to measure the temporal resolution of a gated x-ray detector such as an x-ray framing camera. The picosecond light pulses both drive the XRDS and optically trigger the camera. The frame duration of ~50 psec is simply measured by monitoring the integrated response of the camera as the relative delay between the x-ray pulse and the trigger pulse is varied.

Conclusion.

The x-ray diode source (XRDS) has been developed and characterized. Two XRDS's have been fabricated, incorporating titanium and gold anodes respectively, which exhibit characteristic line and bremstrahlung x-ray emission in the energy range of 2-10 keV. The maximum brightness of the XRDS is $\sim 10^{12}$ phot/sec-cm^2-srad and the source spot size can be varied from a minimum of ~40 microns to 1 cm. The outstanding performance and simple operation of the XRDS makes it an attractive alternative to conventional x-ray sources in many laboratory applications. Furthermore the XRDS provides the unique capability of producing x-ray output with arbitrary, controlled spatial and temporal structure. Future applications of the XRDS include coded imaging using complex x-ray source patterns, phase-sensitive x-ray measurements and the generation of ultra-fast x-ray pulses.

Acknowledgments.

It is a pleasure to acknowledge R. Price (currently at Los Alamos National Laboratory) as the inventor of the x-ray diode source. J. Wiedwald and D. Lord have been major contributors in the design and development of the XRDS. I would like to acknowledge S. Patton of ITT for his assistance in the fabrication of the XRDS. I wish to acknowledge our collaborators on the design and development of the x-ray CCD camera: G. Ricker, J. Doty, J. Vallerga and G. Luppino of the MIT Center for Space Research. Finally, I thank G. Howe and W. Cook for their invaluable assistance in the characterization of the XRDS.

References.

1. Ceglio, N. M., X-ray Microscopy, ed. by G. Schmahl and D. Rudolph (Springer-Verlag, Berlin), 43, 97 (1984).
2. The number of electrons N produced by an x-ray of energy E eV is approximately given by N = E/3.6.
3. Eberhardt, E. H., Applied Optics, 16, 2127 (1977).
4. Gaines, J. L., Nucl. Inst. and Methods, 102, 7 (1972).
5. Barrett, H. H., Garewal, K. and Wilson D. T., Radiology, 104, 429 (1972); Stoner, W. W., Sage, J. P., Braun, M., Wilson, D. T. and Barrett, H. H., Proc. of ERDA Symposium on X-ray and Gamma-ray Sources and Applications, CONF-760539, May 1976.

Table Captions.

1. A comparison of the XRDS and a conventional electron-bombardment x-ray source.

Figure Captions.

1. A schematic depiction of the XRDS.
2. The configuration of the XRDS test station.
3. The calculated x-ray detection efficiency of the CCD camera. The efficiency is the product of the probability of x-ray transmission through the gate structure and oxide layer on the surface of the CCD, and the probability of absorption within the depletion region.

4a. The x-ray emission spectrum of the titanium-anode XRDS operated at 10 kV.

b. The x-ray emission spectrum of the gold-anode XRDS operated at 10 kV.

5a. A pinhole image of the XRDS source spot generated by projecting a 25 micron light spot onto the photocathode.

b. A lineout across a diameter of the pinhole image. The dashed line is a theoretical fit with σ = 20 microns.

6. A schematic illustration of several future applications of the XRDS:

a. Coded imaging is possible by generating a complex x-ray source pattern.

b. Phase-sensitive x-ray measurements can be performed by temporally modulating the input light signal.

c. The production of picosecond x-ray pulses makes it possible to calibrate gated x-ray diagnostics such as the x-ray framing camera.

	Max brightness (Phot/ s - cm^2 - srad)	Min. source size (μm)	Typical power (w)	Water-cooling
XRDS	10^{12}	<40	0.1 - 1	No
Conventional source	10^{14}	~ 3000	1000 - 5000	Yes

Table 1

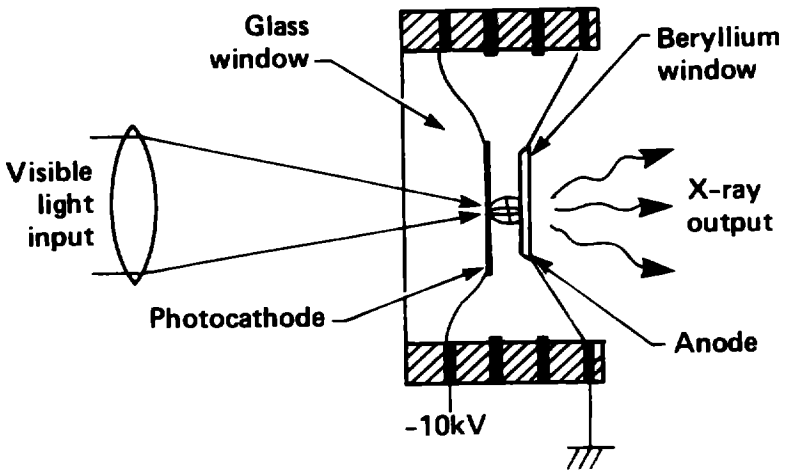
Glass
window
Beryllium
window
Visible
light
input
X-ray
output
Photocathode
Anode
-10kV

Fig. 1

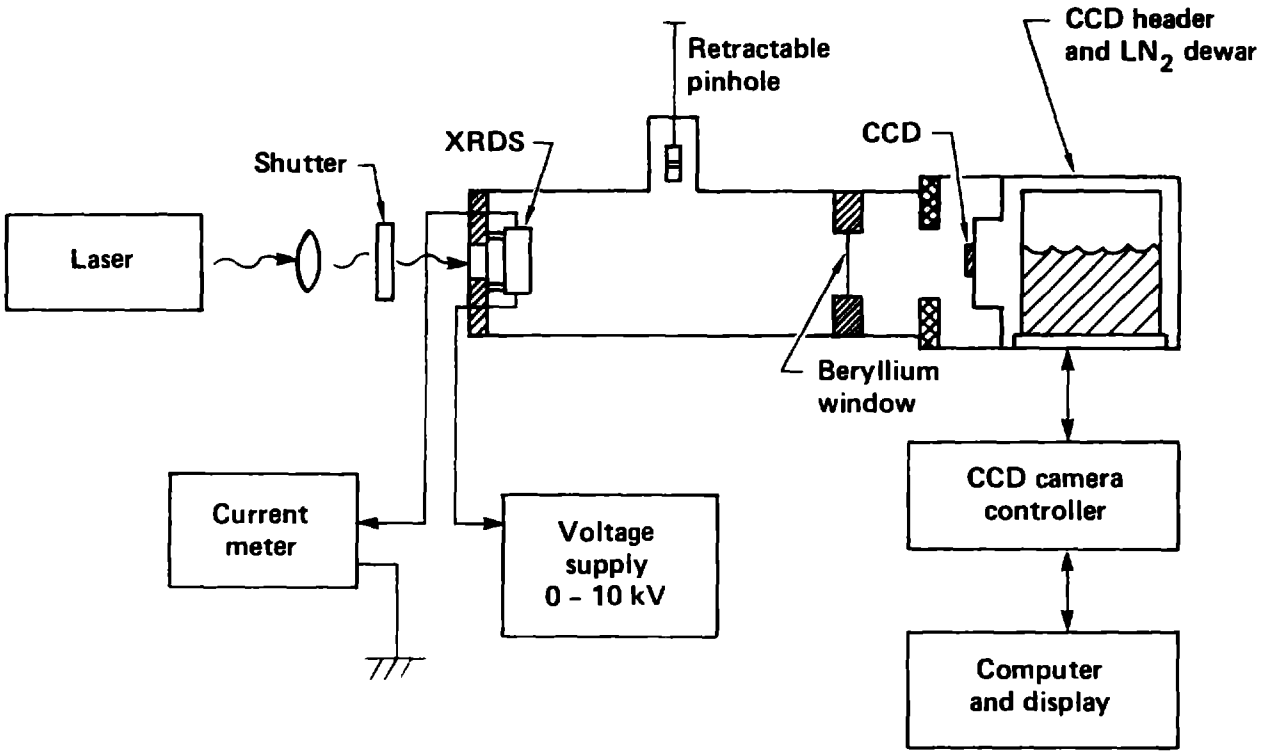
Retractable
pinhole
CCD header
and LN_2 dewar
XRDS
CCD
Shutter
Laser
Beryllium
window
CCD camera
controller
Current
meter
Voltage
supply
0 - 10 kV
Computer
and display

Fig. 2

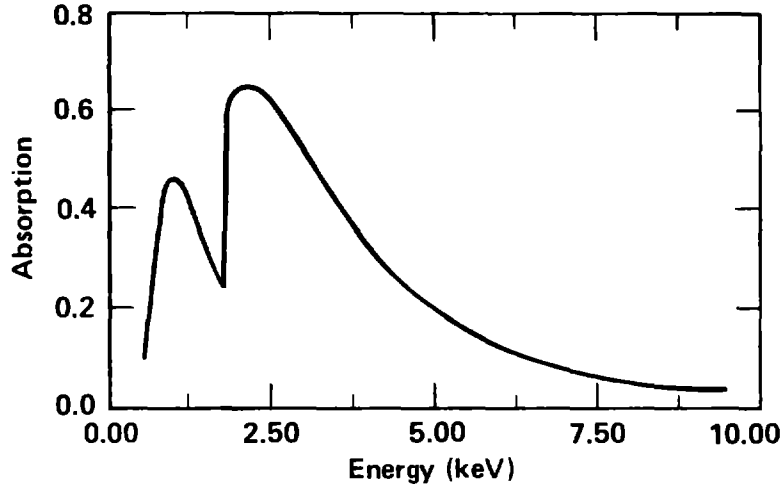

Fig. 3

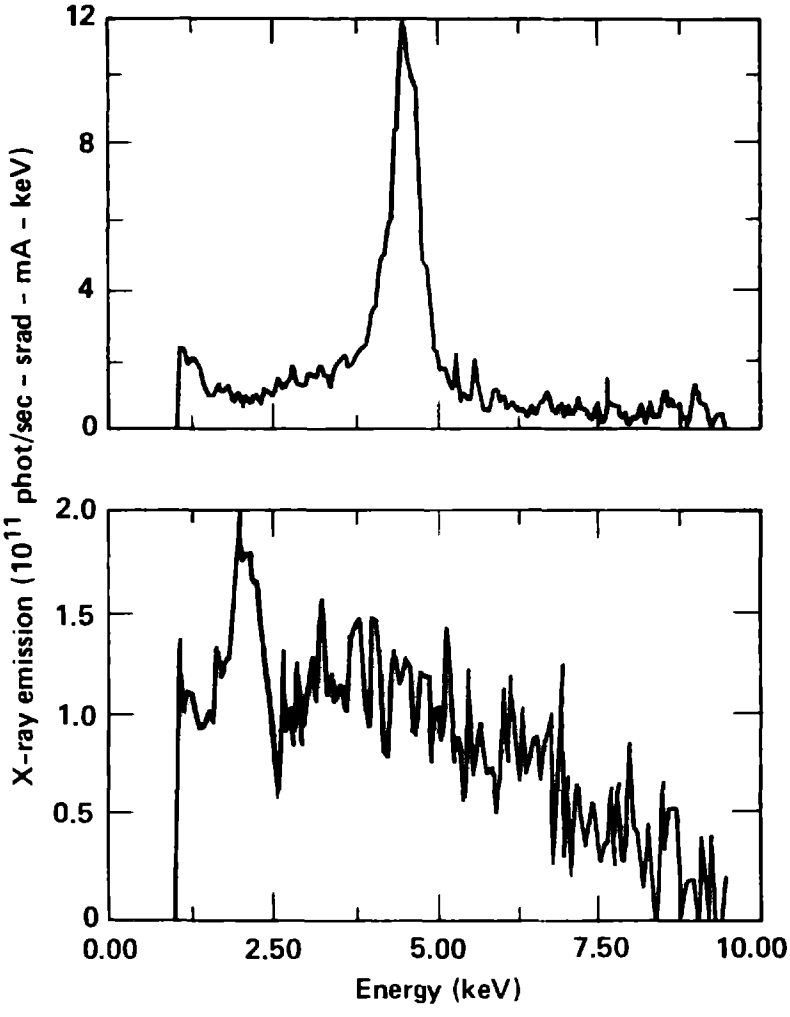
12
8
4
0
2.0
1.5
1.0
0.5
0
X-ray emission (10^{11} phot/sec - srad - mA - keV)
0.00
2.50
5.00
7.50
10.00
Energy (keV)

Fig. 4

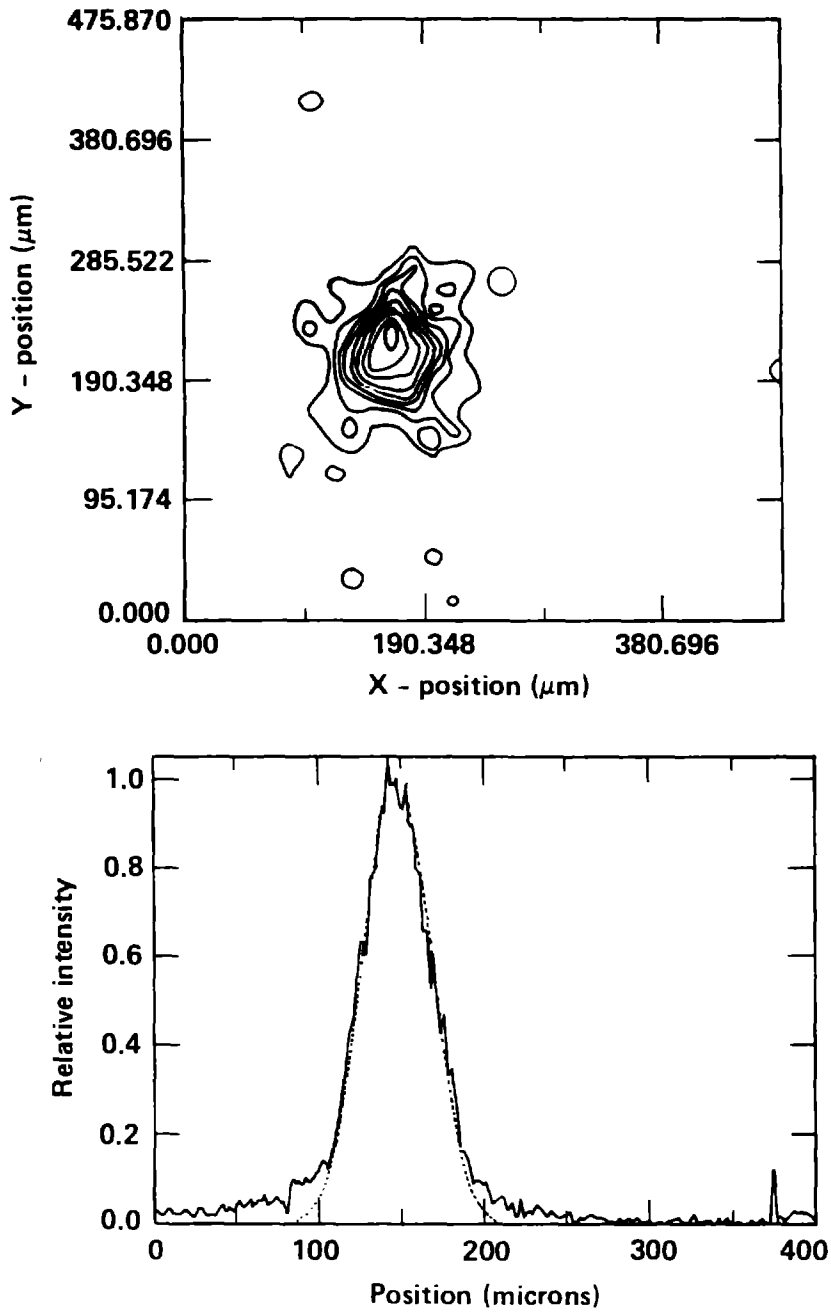
475.870
380.696
285.522
190.348
95.174
0.000
Y - position (μm)
0.000
190.348
380.696
X - position (μm)
1.0
0.8
0.6
0.4
0.2
0.0
Relative intensity
0
100
200
300
400
Position (microns)

Fig. 5

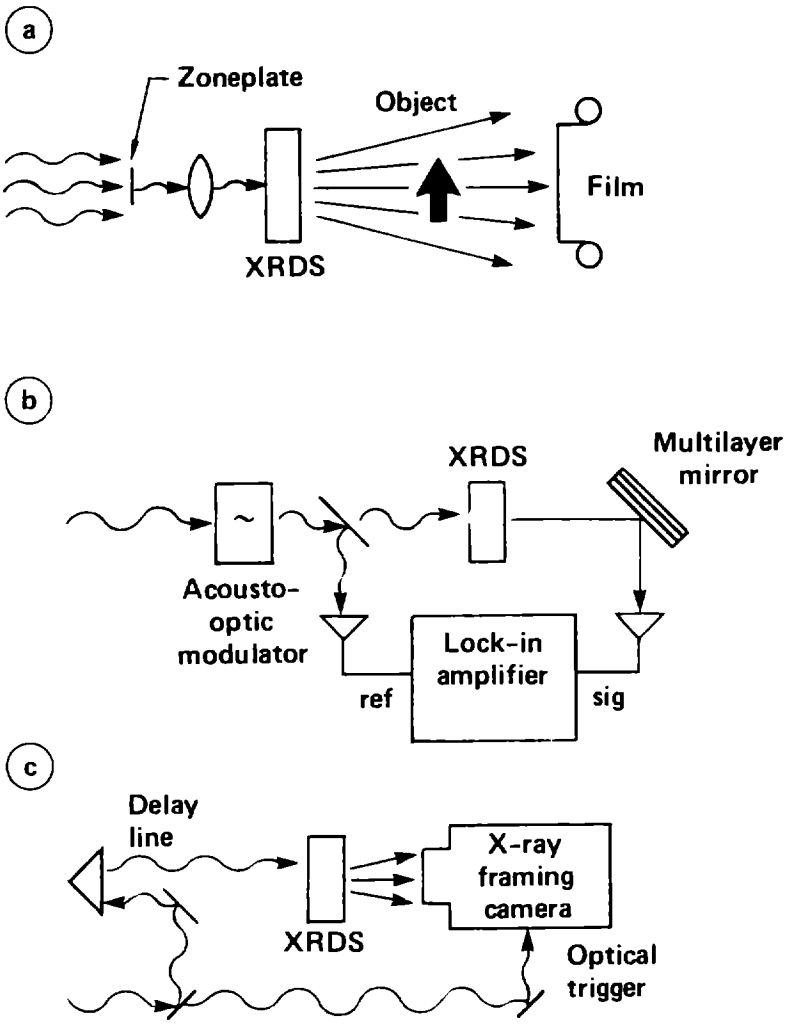
a
Zoneplate
Object
Film
XRDS
b
XRDS
Multilayer
mirror
Acousto-
optic
modulator
Lock-in
amplifier
ref
sig
c
Delay
line
X-ray
framing
camera
XRDS
Optical
trigger

Fig. 6